Inorganic Chemistry

Article

pubs.acs.org/IC

Encapsulation and Sensitization of UV−vis and Near Infrared Lanthanide Hydrate Emitters for Dual- and Bimodal-Emissions in Both Air and Aqueous Media Based on a Porous Heteroatom-Rich Cd(II)-Framework

Yan-An Li,[†] Shu-Kui Ren,[†] Qi-Kui Liu,[†] Jian-Ping Ma,[†] Xueyuan Chen,[‡] Haomiao Zhu,[‡] and Yu-Bin Dong*[,†]

[†]College of Chemistry, Chemical Engineering and Materials Science, Key Laboratory of Molecular and Nano Probes, Engineering Research Center of Pesticide and Medicine Intermediate Clean Production, Ministry of Education, Shandong Provincial Key Laboratory of Clean Production of Fine Chemicals, Shandong Normal University, Jinan 250014, P.R. China

[‡]State Key Laboratory of Structural Chemistry, Fujian Institute of Research on the Structure of Matter, Chinese Academy of Science, Fuzhou, Fujian 350002, P.R. China

Supporting Information

ABSTRACT: A porous heteroatom-rich Cd(II)-polymeric framework which is generated from an ethylene glycol ether-bridging dicarboxylate ligand **L**, 4,4′-bipy and Cd(II) ion is reported. It contains one-dimensional tubes (9−11 Å) which are able to trap cationic lanthanide hydrates such as $Eu(H_2O)_8^{3+}$, $Tb(H_2O)_8^{3+}$, and $Nd(H_2O)_8^{3+}$ under ambient conditions to generate $Ln(H_2O)_8^{3+}$-loaded materials. In addition, the heteroatom-rich host material can effectively protect and sensitize the encapsulated Ln^{3+} emitters in their hydrate form in both air and aqueous media. Furthermore, the dual- and bimodal-emissions are successfully realized by intercalation of the different Ln^{3+}-hydrates based on a guest-driven approach.

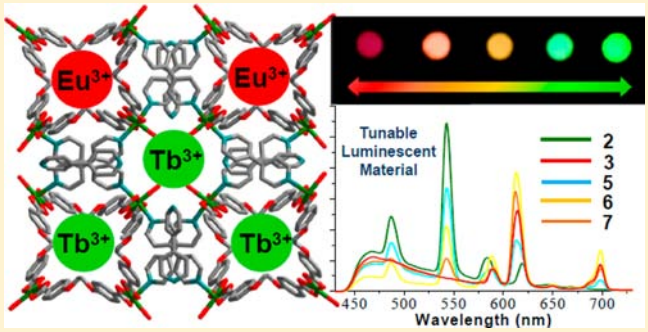

INTRODUCTION

For access to the dual-emission and bimodal emission materials, significant effort has been dedicated to the design and synthesis of the heterolanthanide cocktails.[1] However, the preparation of *f*-*f* hybrids are very difficult because of the inherent disadvantage in the synthesis of the organic ligands with specific recognizing sites required by the different lanthanide cations.

Metal−organic frameworks (MOFs),[2] as a new class of porous materials, provide a new chemical phase which consists of both inorganic and organic components. In principle, their interior microenvironment could be modified by simply changing the functional organic spacers, metal nodes, and sometimes counterions. Such advantages endow MOFs with a variety of physicochemical properties. Most of the functionalities derive from MOFs basically based on their ability to recognize specific guest substrates through elusive host−guest interactions. Among various MOFs, the porous heteroatom-rich MOFs with a hydrophilic internal surface provide a novel platform to generate new functionality, for example, trapping electrophilic species into pores. With this in mind, we have initiated a synthetic program for preparation of the porous heteroatom-rich MOFs, in which the flexible open-chain polyether-bridged organic spacers are chosen as the building blocks.[3]

In this contribution, we present a neutral porous three-dimensional Cd(II)-MOF which has a perfect pore size for trapping lanthanide hydrates. The Cd(II)-MOF herein can effectively protect and sensitize the Ln^{3+} hydrate emitting in the UV−vis and Near Infrared (NIR) ranges in both air and aqueous media. Furthermore, the dual- and bimodal-emissions are successfully realized based on the reversible heterolanthanide cationic species encapsulation.

RESULTS AND DISCUSSIONS

Synthesis and Characterization of Heteroatom-Rich Cd(II)-MOF. Compound **1** ($[Cd(4,4'\text{-bipy})(H_2O)(\mathbf{L})]\cdot(4,4'\text{-bipy})\cdot 11(H_2O)$) was obtained as rod-like colorless crystals by the combination of flexible ethylene glycol ether bridging bicarboxylate ligand **L** and rigid 4,4′-bipyridine with $Cd(OAc)_2$ under hydrothermal conditions (Figure 1). The single-crystal analysis revealed that **1** crystallizes in the tetragonal space group *P*4(1)2(1)2 (Table 1). As shown in Figure 1, the Cd(II) nodes extend along the crystallographic *c* axis through **L** to form a single-stranded helix with a period of separation of 69.439 Å. It is

Received: March 30, 2012
Published: August 23, 2012

   dx.doi.org/10.1021/ic300665a | *Inorg. Chem.* 2012, 51, 9629−9635

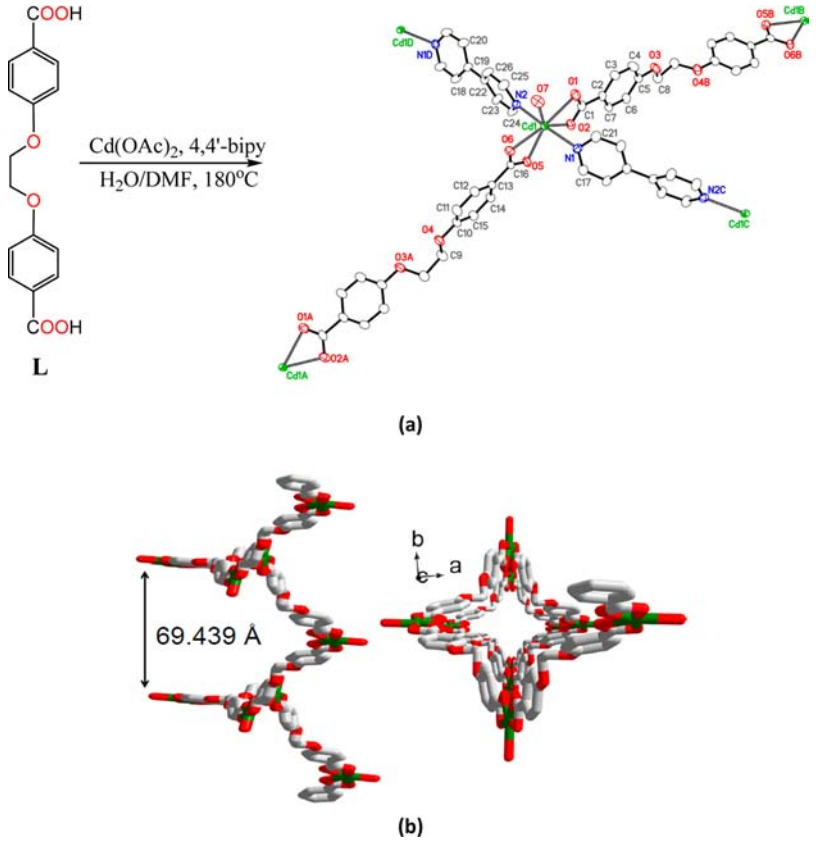

Figure 1. (a) Synthesis of **1** and its Cd(II) coordination sphere. (b) Single helical **L**-Cd(II) chain.

Table 1. Crystal Data and Structure Refinement for 1

identification code	**1**
empirical formula	$C_{62}H_{74}Cd_2N_6O_{25}$
formula weight	1528.07
temperature	123(2) K
wavelength	0.71073 Å
crystal system, space group	tetragonal, $P4(1)2(1)2$
unit cell dimensions	a = 22.5663(14) Å
	α = 90°
	b = 22.5663(14) Å
	β = 90°
	c = 13.8877(18) Å
	γ = 90°
volume	7072.1(11) Å^3
Z, calculated density	4, 1.435 Mg/m^3
absorption coefficient	0.682 mm^{-1}
$F(000)$	3136
crystal size	0.45 × 0.13 × 0.13 mm
θ range for data collection	1.28 to 25.60 deg
limiting indices	$-15 \le h \le 27$
	$-27 \le k \le 26$
	$-16 \le l \le 16$
reflections collected/unique	37637/6668 [R(int) = 0.0403]
completeness to θ = 25.60	100.0%
absorption correction	semiempirical from equivalents
max. and min. transmission	0.9166 and 0.7490
refinement method	full-matrix least-squares on F^2
data/restraints/parameters	6668/12/444
goodness-of-fit on $\hat{F}^2$	1.106
final R indices [$I > 2\sigma(I)$]	R1 = 0.0378, wR2 = 0.0933
R indices (all data)	R1 = 0.0399, wR2 = 0.0945

noteworthy that five such Cd(II)-**L** helical chains in **1** interwine with each other to form a one-dimensional (1D) tube, in which the shortest aromatic C···C distance between neighbor chains is 3.8 Å (Figure 2a). As shown in Figure 2a, each tube features a distorted square-like channel and is surrounded by oxygen atoms. The opposite O···O separations on the ethylene glycol ether lie in a range of 9−12 Å, while the diagonal carboxylate O···O distances are 10−11 Å. We find it noteworthy that all chains within the tube have the same handedness (*P*-helix), leading to an overall chiral structure. Furthermore, these 1D tubes are cross-linked by 4,4′-bipy coligands to provide a novel noninterpenetrating three-dimensional porous framework (Figure 2b). In addition, the packing of adjacent tubes along the crystallographic *c* axis also leads to an open octagonal channel of about 9 × 11 Å (Figure 2b). Interestingly, one uncoordinated 4,4′-bipy per formula exists in the lattice. They are symmetrically around the octagonal channels and face toward the center of the channel with a N···N distance of ∼11 Å. Moreover, the coordinated aquo oxygen atoms also face to the center of the channels with a opposite O···O distance of ∼ 9 Å. As shown in Figure 2b, both two types of channels are filled with water guest molecules, which is further confirmed by thermogravimetric analysis (TGA) (Supporting Information). The encapsulated water molecules form two types of *P*-helical water chains within these right-handed channels, respectively (Supporting Information). The formation of *P*-type water-helices are clearly induced by the *P*-helical channels. The average O···O distance within the water chain in the distorted square-like channel is 2.684 Å, while the average O···O separation of the water chain in an octagonal channel is 2.605 Å. The average O···O distances herein are significantly shorter than those of ice[4] which might result from the strong confined space effect.

dx.doi.org/10.1021/ic300665a | *Inorg. Chem.* 2012, 51, 9629−9635

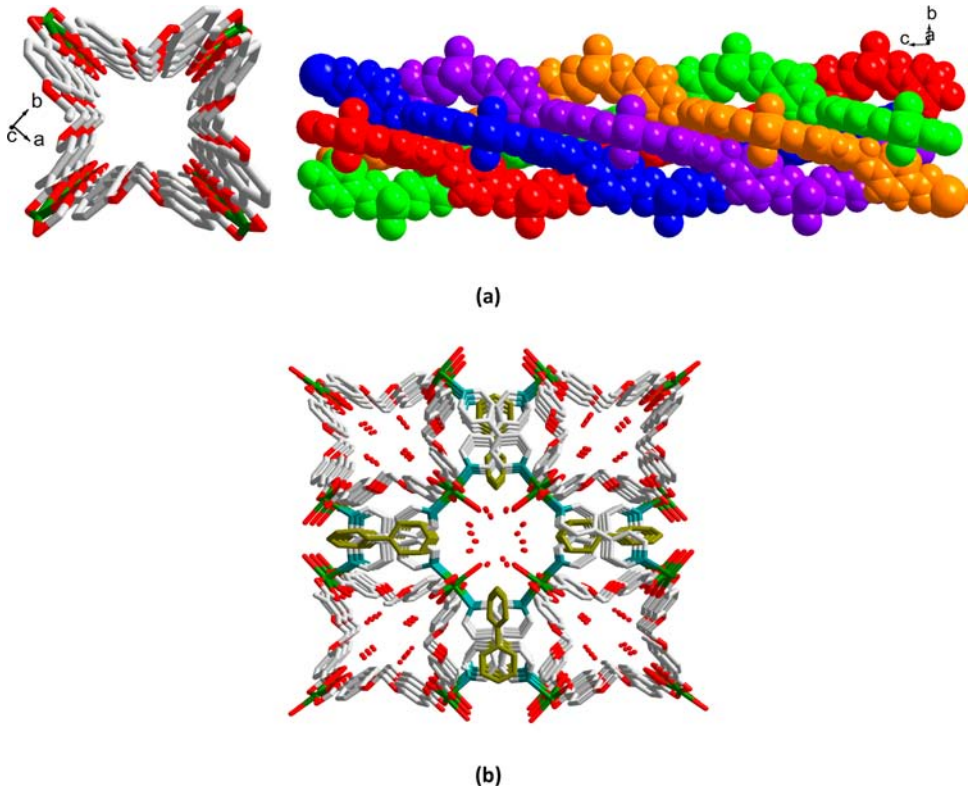

Figure 2. (a) Top and side views (shown in different colors for clarity) of five Cd(II)-**L** strands interwine with each other to generate 1D tube extended along the crystallographic *c* axis. (b) Oxygen-rich 1D tubes are cross-linked by 4,4′-bipy to generate a noninterpenetrating three-dimensional framework. As shown in the structure, there are two types of tubes in **1** which are filled with water guest molecules. The uncoordinated 4,4′-bipy are highlighted in yellow-brown for clarity.

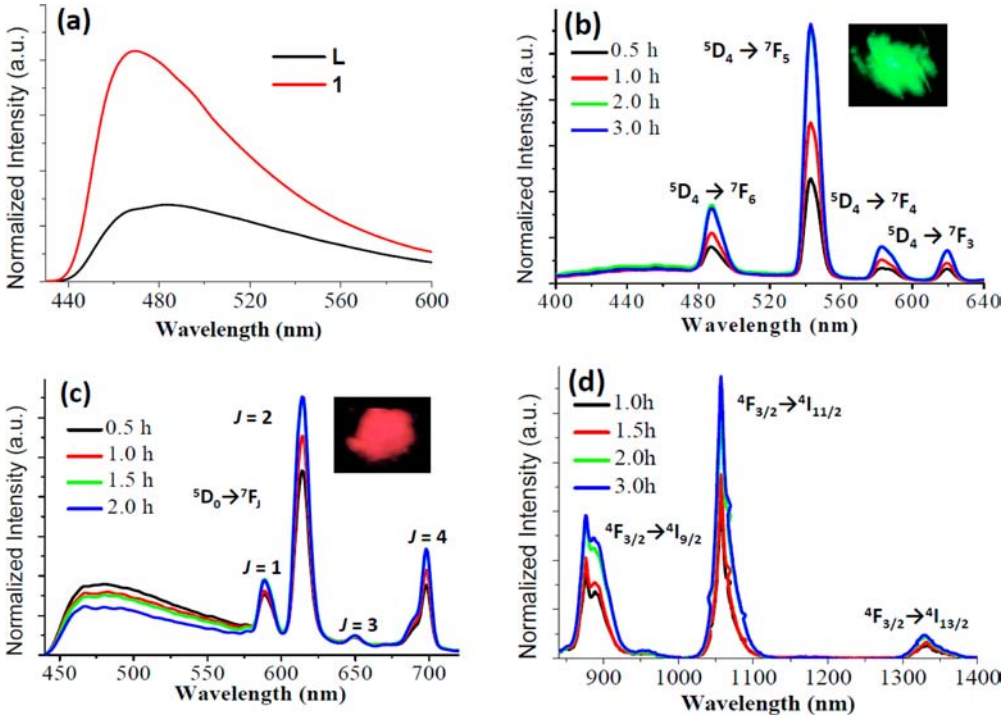

Figure 3. Solid-state emission spectra measured in air of (a) **L** and **1**. (b) **1** immersed in an aqueous solution of $Tb(ClO_4)_3$ (2.0%) during 0.5−2.0 h (λ_{ex} = 323 nm). (c) **1** immersed in an aqueous solution of $Eu(ClO_4)_3$ (2.0%) during 0.5−3.0 h (λ_{ex} = 395 nm). (d) **1** immersed in an aqueous solution of $Nd(ClO_4)_3$ (2.0%) during 1.0−3.0 h (λ_{ex} = 750 nm). The samples of **2** and **3** illuminated with 254 nm laboratory UV light are inserted.

Encapsulation and Sensitization of Lanthanide Hydrate Emitters. It is worthy to note that **1** is luminescent. Upon excitation at 340 nm, **1** emits strong blue light with an emission maximum at 458 nm (Figure 3a), at which bilirubin is broken

dx.doi.org/10.1021/ic300665a | *Inorg. Chem.* 2012, 51, 9629−9635

down.[5] So **1** might have potential application in phototherapy to treat newborn jaundice by destruction of bilirubin.[5] Compared to the ligand emission (483 nm), the emission intensity of **1** is significantly enhanced, and the blue-shift luminescence of **1** is believed to be based upon ligand-to-metal-charge-transfer (LMCT). As shown above, the cavity sizes of two types of hydrophilic channels are in the range of 9−11 Å, which are perfect dimensions for trapping $[Ln(H_2O)_8]^{3+}$ through hydrogen bonding interactions.[3b,6] With this in mind, the Ln^{3+} hydrate adsorption experiments were carried out based on **1** (Scheme 1).

Scheme 1. Ln(III)-Hydrate Encapsulation Based on 1 in Aqueous Solution

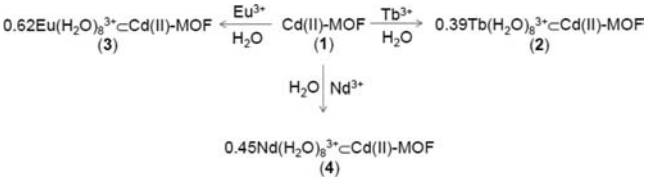

As expected, when **1** was immersed in an aqueous solution of $Tb(ClO_4)_3$ (2.0%), the solid-state photoinduced-emission monitoring indicates that the $Tb(H_2O)_8^{3+}$ was trapped (Scheme 1). The maximal emission intensity of Tb^{3+} was obtained after 2 h. Four typical lines of Tb^{3+} emission were detected in the visible spectrum (Figure 3b), corresponding to transitions from the $^5D_4$ state: $^5D_4 \rightarrow {}^7F_6$ (487 nm), $^5D_4 \rightarrow {}^7F_5$ (543 nm), $^5D_4 \rightarrow {}^7F_4$ (583 nm), $^5D_4 \rightarrow {}^7F_3$ (619 nm). The most prominent line was observed at 543 nm. The ICP (Inductively Coupled Plasma) measurement (Supporting Information) indicates that the doped amount of Tb^{3+} is up to 6.74% and afford **0.39Tb$(H_2O)_8^{3+}$⊂Cd-(II)-MOF** (**2**). In a similar way, an $Eu(H_2O)_8^{3+}$-loaded sample was obatined by immersing **1** in a 2.0% aqueous solution of $Eu(ClO_4)_3$ for 1.5 h (Scheme 1). As shown in Figure 3c, the emission bands of Eu^{3+} arise from the $^5D_0 \rightarrow {}^7F_J$ (J = 1, 2, 3, 4) transitions of Eu^{3+}. The corresponding emission bands are 589, 614, 650 and 698 nm, respectively. Among these transitions, $^5D_0 \rightarrow {}^7F_2$ is the strongest. The ICP measurement (Supporting Information) indicates that the doped amount of Eu^{3+} is up to 9.89% to afford **0.62Eu$(H_2O)_8^{3+}$⊂Cd(II)-MOF** (**3**). As shown in Figure 3b−c, when the samples of **2** and **3** were excited with a UV lamp (254 nm), the terbium and europium emitted their distinctive colors which were readily observed with the naked eye.

Besides UV−vis emitters, the NIR-lanthanide emitter such as Nd^{3+} can also be trapped by **1** (Scheme 1). For example, the crystals of **1** were immersed in an aqueous solution of $Nd(ClO_4)_3$ (2.0%) at ambient temperature for 3 h, generating a Nd-$(H_2O)_8^{3+}$-loaded sample. As shown in Figure 3d, emission bands are observed at 876, 1057, and 1330 nm which are attributed to the $^4F_{3/2} \rightarrow {}^4I_{9/2}$, $^4F_{3/2} \rightarrow {}^4I_{11/2}$, and $^4F_{3/2} \rightarrow {}^4I_{13/2}$ transitions, respectively. The ICP measurement (Supporting Information) indicates that the doped amount of Nd^{3+} is up to 8.01%, which suggests the formation of **0.45Nd$(H_2O)_8^{3+}$⊂Cd(II)-MOF** (**4**).

The XRD patterns of the $Eu(H_2O)_8^{3+}$, $Tb(H_2O)_8^{3+}$, and $Nd(H_2O)_8^{3+}$-loaded samples (**2**−**4**) confirm that the structure of **1** is maintained upon the lanthanide hydrates' adsorption (Figure 4).

Guest-Driven Tunable Luminescent Properties. *Tunable Luminescence within UV−vis Region in Air.* Interestingly, this heteroatom rich host is able to successively incorporate different Ln^{3+} cationic species into a single host framework to

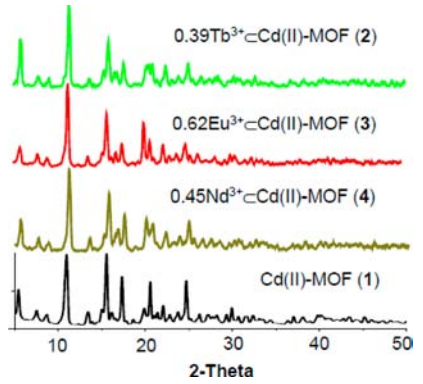

Figure 4. XRPD patterns of **1**−**4**.

form a heterometallic host−guest system, furthermore, simultaneously sensitize their emissions to exhibit dual-emission. For example, when **0.39Tb$(H_2O)_8^{3+}$⊂Cd(II)-MOF** (**2**) was treated with $Eu(ClO_4)_3$ (2.0%) in water for 10 min (Scheme 2), the

Scheme 2. Heterometallic Tb/Eu(III)-Hydrates Encapsulation Based on 2 in Aqueous Solution

emission spectra (λ_{ex} = 360 nm) indicated that both $Tb(H_2O)_8^{3+}$ and $Eu(H_2O)_8^{3+}$ were incorporated to generate a heterolanthanide cocktail (Figure 5). ICP analysis (Supporting Information) indicates the absorbed amount of europium is up to 2.67%, while the encapsulated amount of terbium is basically unchanged (6.53%) to give rise to **0.37Tb$(H_2O)_8^{3+}$/0.16Eu$(H_2O)_8^{3+}$⊂Cd-(II)-MOF** (**5**). No more changes for the luminescent intensities have been observed in the emission spectrum after 2 h. Compared to **5**, the doped amount (based on ICP analysis, Supporting Information) of europium further enhanced (9.05%), and the amount of terbium correspondingly reduced (4.12%), which suggests the formation of **0.28Tb$(H_2O)_8^{3+}$/0.65Eu$(H_2O)_8^{3+}$⊂Cd(II)-MOF** (**6**) at 2 h (Scheme 2). So the incorporated terbium cationic species were partly replaced by the incoming europium cationic species at 2 h. Reasonably, the typical Eu^{3+} emission bands increased at the expense of Tb^{3+} emission as time went on, which was well demonstrated by their emission spectra (Figure 5).

Notably, the encapsulated $Ln(H_2O)_8^{3+}$ can be reversibly displaced, and the Eu^{3+}/Tb^{3+} cocktail can also be obtained based on **0.62Eu$(H_2O)_8^{3+}$⊂Cd(II)-MOF** (**3**) (Scheme 3). For example, treatment of **3** with $Tb(ClO_4)_3$ in aqueous solution (2%) for 10 min, resulting in the formation of heterometallic host−guest system **0.32Eu$(H_2O)_8^{3+}$/0.20Tb$(H_2O)_8^{3+}$⊂Cd-MOF** (**7**) (europium: 5.61%; terbium: 3.23%, based on ICP analysis, Supporting Information). Compared to **5** and **6**, the codoped Cd(II)-MOF material of **7** displays the different relative Eu^{3+}/Tb^{3+} emission intensities (Figure 5) caused by the different encapsulated Eu^{3+}/Tb^{3+} molar ratios. The naked eye detectable colors of $Tb(H_2O)_8^{3+}/Eu(H_2O)_8^{3+}$⊂Cd(II)-MOF samples illuminated with 254 nm laboratory UV light objectively reflect the changes of their emission spectra. As shown in Figure 5, samples of **2**−**7** successively exhibit green, cyan, yellow, pink and red colors which are driven by the doped relative Eu^{3+}/Tb^{3+}

dx.doi.org/10.1021/ic300665a | Inorg. Chem. 2012, 51, 9629−9635

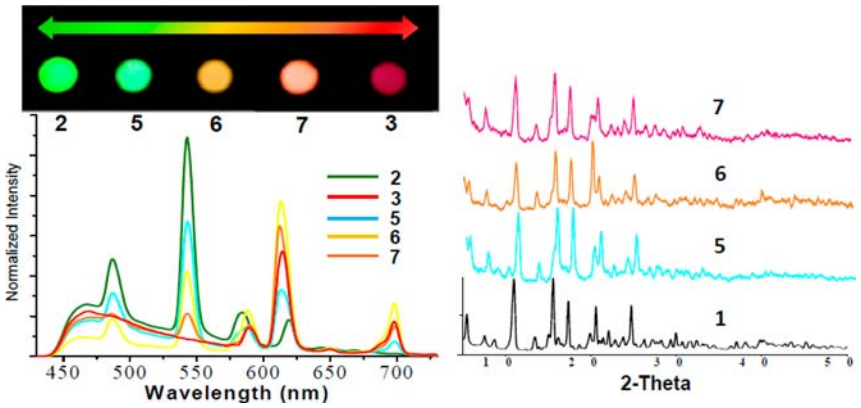

Figure 5. Left: Solid-state emission spectra of **2**, **3**, **5**, **6**, and **7** (λ_{ex} = 360 nm). The samples of **2**, **3**, **5**, **6**, and **7** illuminated with 254 nm laboratory UV light are inserted. Right: The corresponding XRPD patterns of **5**−**7** and as-synthesized of **1**.

Scheme 3. Heterometallic Eu/Tb(III)-Hydrates Encapsulation Based on 3 in Aqueous Solution

$$0.62Eu(H_2O)_8^{3+}\subset Cd(II)\text{-MOF}\ (\mathbf{3}) \xrightarrow[H_2O]{Tb^{3+}} 0.32Eu(H_2O)_8^{3+}/0.20Tb(H_2O)_8^{3+}\subset Cd(II)\text{-MOF}\ (\mathbf{7})$$

percentage. In principle, the stoichiometry of the codoped bis-lanthanide in Cd(II)-MOF is not restricted, so the composition of the cocktail can be easily tuned depending on the inherent bias of the MOF antenna chromophore to sensitize Eu^{3+} and Tb^{3+} emissions with comparable sensitivity. Such multiband emissions from the heterolanthanide doped Cd(II)-MOFs might be a bar-coded luminescent materials. The XRPD patterns on resulted heterometallic materials of **5**−**7** are identical to that of **1**, so the framework is stable during the different lanthanide species adsorption (Figure 5).

Tunable Luminescence between UV−vis and NIR Regions in Air. Besides UV−vis emitters, **1** can also the encapsulated both UV−vis and NIR emitters such as terbium and neodymium. For example, treatment of **0.39Tb$(H_2O)_8^{3+}\subset$Cd(II)-MOF** (**2**) with an aqueous solution of $Nd(ClO_4)_3$ (2.0%) resulted in the formation of UV−vis/NIR cocktail (Scheme 4). As shown in

Scheme 4. Heterometallic Tb/Eu(III)-Hydrates Encapsulation Based on 2 in Aqueous Solution

$$0.39Tb(H_2O)_8^{3+}\subset Cd(II)\text{-MOF}\ (\mathbf{2}) \xrightarrow[H_2O]{Nd^{3+}} 0.31Tb(H_2O)_8^{3+}/0.34Nd(H_2O)_8^{3+}\subset Cd(II)\text{-MOF}\ (\mathbf{8})$$

Figure 6, the typical Nd^{3+} emission bands in the NIR region increased as the adsorption process going on. After 8 h, the adsorption is finished depending on the emission spectral monitor. The slightly decreased emission from Tb^{3+} which might be resulted from that the partial encapsulated Tb^{3+} cations were replaced by Nd^{3+}, which is further confirmed by ICP-LC. The ICP analysis (Supporting Information) indicates that the residual Tb^{3+} is 5.67% and corresponding adsorbed amount of Nd^{3+} is up to 5.54% to provide **0.31Tb$(H_2O)_8^{3+}$/0.34Nd$(H_2O)_8^{3+}\subset$Cd-MOF** (**8**). So the adsorption of Tb^{3+} and Nd^{3+} by Cd(II)-MOF did lead to the tunable emission between UV−vis and NIR regions, that is, the bimodal-emission upon being excited at different wavelengths. Again, the X-ray powder diffraction (XRPD) monitoring confirms that the original structure remains intact during the course of the reaction (Figure 6).

As shown above, lanthanide hydrate cationic species are inserted into a neutral network of **1**, so the corresponding anionic species should be encapsulated for the charge compensation. The X-ray photoelectron spectroscopy (XPS) observations of Cl 2p peaks in **2**−**8** (Supporting Information) supported well the coexistence of the ClO_4^- anion. To further confirm the encapsulated lanthanide species in **1** to be the hydrate form, thermogravimetric analyses were carried out on the samples of **2**−**8** (Supporting Information). TGA traces showed a gradual weight-loss step (below 150 °C) of 12.9% for **2**, (calcd. 13.3%), 17.3% for **3** (calcd. 16.4%), 12.1% for **4** (calcd. 11.9%), 11.2% for **5** (calcd. 10.1%), 18.7% for **6** (calcd. 18.5%), 10.5% for **7** (calcd.

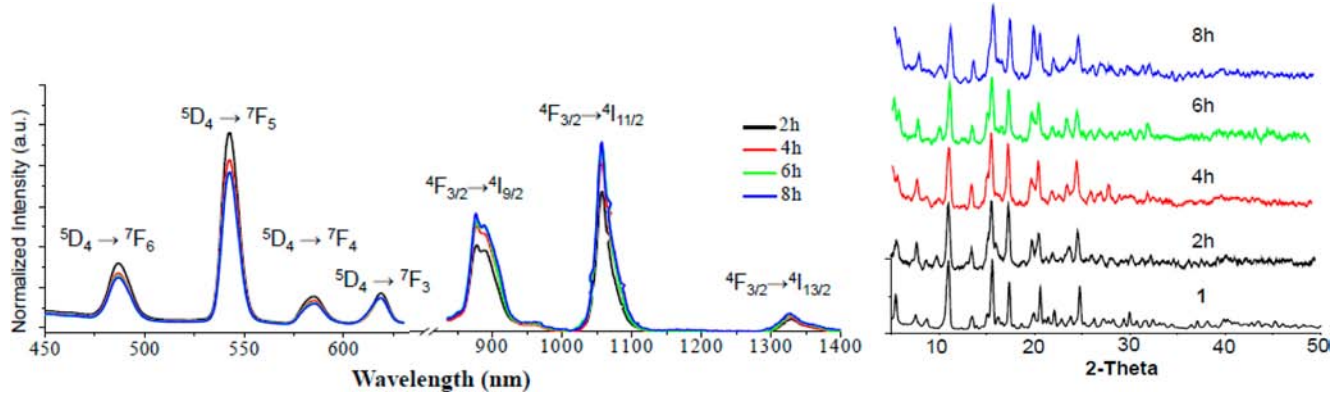

Figure 6. Left: Solid-state emission spectra of **2** immersed in a 2.0% aqueous solution of Nd^{3+} at 2.0−8.0 h. As time went on, the emission intensities of Tb^{3+} gradually decreased (λ_{ex} = 323 nm), while the emission intensity of Nd^{3+} correspondingly increased (λ_{ex} = 750 nm). Right: Corresponding XRPD patterns.

dx.doi.org/10.1021/ic300665a | *Inorg. Chem.* 2012, 51, 9629−9635

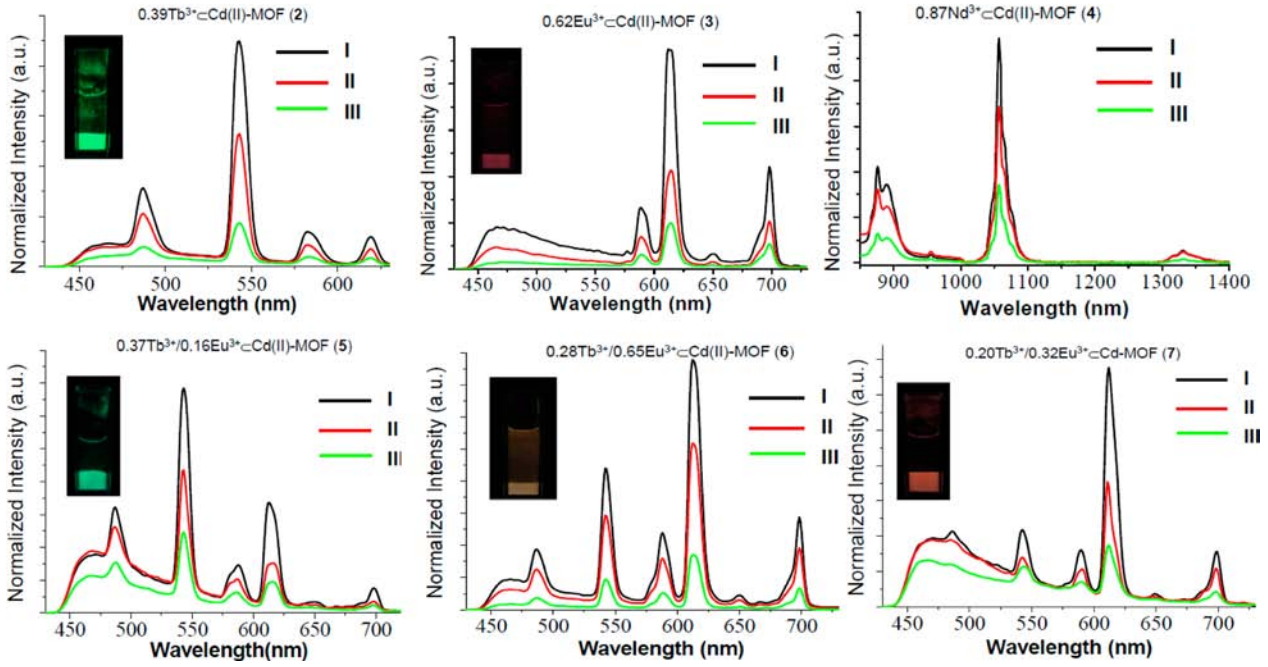

Figure 7. Photoinduced emission spectra of **2**–**7** measured in air (I), moistened by water (II) and completely immersed in water (III). The samples of **2**, **3**, **5**, **6**, and **7** in water illuminated with UV light (254 nm) are inserted.

9.9%), and 14.7% for **8** (calcd. 14.5%), respectively, corresponding to escape of the water guest molecules. In addition, the IR spectra performed on **2**–**8** also confirmed the existence of water molecules (Supporting Information). It is well-known that the hydration states of the lanthanide complexes have a very significant effect on their metal-centered luminescent behaviors resulted from the O-H vibrational quenching.[7] The intense emission of $Ln(H_2O)_8^{3+}$ herein reasonably indicates that the strong coupling of O-H vibrations on the coordinated water molecules is efficiently reduced within the heteroatom-rich cavities by the interhost–guest O-H···O and O-H···N H-bonding interactions. Besides our research group,[6] some tunable luminescent MOFs based on reversible Ln^{3+} encapsulation have been reported very recently by others; the lanthanide species loading therein, however, was carried out in DMF solution in nonhydrate form.[8] Lanthanide hydrate species loading in aqueous solution based on porous heteroatom-rich MOFs herein effectively expands the scope of guest-driven lanthanide luminescent materials.

Luminescence in Water. To evaluate the protecting and sensitizing ability of Cd(II)-MOF in an aqueous medium, the luminescent properties of $[Ln(H_2O)_8]^{3+}$⊂Cd(II)-MOF (**2**–**4**) and $[Ln/Ln'(H_2O)_8]^{3+}$⊂Cd(II)-MOF (**5**–**7**) were tested in water. When the $Ln(H_2O)_8^{3+}$-loaded samples were moistened and completely immersed in water, the corresponding Ln^{3+} emissions were clearly detected (Figure 7). Compared to their luminescent spectra obtained in air, the corresponding emission intensities measured in aqueous medium reduced to some extent, which logically results from the water quenching by the loss of lanthanide sensitization in part. Nevertheless, the Cd(II)-MOF herein effectively protects and sensitizes the UV–vis and NIR Ln^{3+} emitters in aqueous solution.

CONCLUSIONS

In summary, we have described a novel tunable luminescent material based on a porous Cd(II)-MOF by reversible lanthanide encapsulation. The porous heteroatom-rich Cd(II)-MOF is able to trap Eu^{3+} or Tb^{3+} and Eu^{3+}/Tb^{3+} hydrate species and, furthermore, effectively sensitize their emissions in both air and aqueous media under ambient conditions. In addition, the luminescent cocktail emissions can be easily tuned within UV–vis region and between UV–vis/NIR regions by adjusting the ratios of the encapsulated lanthanide emitters. Such guest-driven approach based on MOFs could be a viable approach to access to the "cocktail" optical materials.

EXPERIMENTAL SECTION

Materials and Methods. $Cd(NO_3)_2$ (Acros) was used as obtained without further purification. Infrared (IR) samples were prepared as KBr pellets, and spectra were obtained in the 400–4000 cm^{-1} range using a Perkin-Elmer 1600 FTIR spectrometer. Elemental analyses were performed on a Perkin-Elmer Model 2400 analyzer. ^1H NMR data were collected using an AM-300 spectrometer. Chemical shifts are reported in δ relative to TMS. All fluorescence measurements were carried out on a Cary Eclipse Spectrofluorimeter (Varian, Australia) equipped with a xenon lamp and quartz carrier at room temperature. Thermogravimetric analyses were carried out using a TA Instrument SDT 2960 simultaneous DTA-TGA under flowing nitrogen at a heating rate of 10 °C/min. XRD pattern were obtained on a D8 ADVANCE X-ray powder diffractometer with CuKa radiation (λ = 1.5405 Å). ICP-LC was performed on IRIS Intrepid II XSP and NU AttoM.

Synthesis of L. A mixture of corresponding polyether-bridged bisbenzaldehyde (1.62 g, 6 mmol), MeOH (20 mL), and H_2O_2 (30%, 6 mL) was stirred in a NaOH (40%, 15 mL) aqueous solution at 35 °C for 3 h. After neutralization by HCl, the product was obtained as white solids (87%). IR (KBr pellet cm^{-1}): 2950 (m), 2885 (m), 2558 (m), 1678 (), 1604 (s), 1579 (m), 1513 (m), 1481 (w), 1435 (s), 1300 (s), 1248 (s), 1166 (s), 1117 (w), 1046 (m), 944 (m), 857 (m), 843 (w), 769 (m), 692 (w), 645 (m), 628 (w). ^1H NMR (300 MHz, DMSO-d_6, 25 °C, TMS, ppm): 12.65 (s, 2H, -COOH), 7.91–7.88, 7.08–7.05 (d, d, 8H, -C_6H_4-), 4.41 (s, 4H, -OCH_2CH_2O-). Elemental analysis (%) calcd for $C_{16}H_{14}O_6$: C 63.57, H 4.63; Found: C 63.46, H 4.68.

Synthesis of 1. L (3.7 mg, 0.012 mmol), $Cd(OAc)_2$ (7.5 mg, 0.033 mmol), 4,4′-bipyridine (2.9 mg, 0.018 mmol), and water (2 mL) were sealed in a 5 mL glass tube. The mixture was heated at 150 °C for 2 days under autogenous pressure. After the mixture was allowed to cool to room temperature, colorless rod-like crystals were isolated from the tube

dx.doi.org/10.1021/ic300665a | Inorg. Chem. 2012, 51, 9629–9635

in 36% yield. IR: 3442 (br), 2941 (w), 2882 (w), 2361 (w), 1604 (s), 1547 (s), 1509 (w), 1413 (s), 1339 (w), 1303 (w), 1255 (s), 1219 (w), 1171 (m), 1006 (m), 853 (w), 806 (m), 779 (m), 628 (m). Elemental analysis(%) calcd for $Cd_8H_{160}O_{68}C_{260}N_{16}$: C 56.83, H 2.93, N 4.08; Found: C 56.77, H 2.85, N 4.32.

Typical Homo-Ln^{3+} Adsorption. **1** (25 mg) was immersed in a 2% aqueous solution of $Ln(ClO_4)_3$ (Ln = Tb(III), Eu(III), and Nd(III)). The resultant crystalline solids were collected and washed by water (5 mL × 3) and MeOH (5 mL × 2), Et_2O (5 mL × 1), and dried in air.

Typical Hetero-Ln^{3+}/Ln'^{3+} Adsorption. **$Ln(H_2O)_8^{3+}$⊂Cd(II)-MOF** (25 mg, Ln = Tb^{3+} or Eu^{3+}) was immersed in a 2% aqueous solution of $Ln'(ClO_4)_3$ (Ln = Eu^{3+}, Tb^{3+} or Nd^{3+}). The resultant crystalline solids were collected and washed by water (5 mL × 3) and MeOH (5 mL × 2), Et_2O (5 mL × 1), and dried in air.

Single-Crystal Analysis. $C_{62}H_{74}Cd_2N_6O_{25}$ (**1**), M = 1528.07, tetragonal, space group $P4(1)2(1)2$, a = 22.5663(14) Å, b = 22.5663(14) Å, c = 13.8877(18) Å, V = 7072.1(11) Å^3, Z = 4, D_c = 1.435 g cm^{-3}, $\mu(Mo_{k\alpha})$ = 0.682 mm^{-1}, $F(000)$ = 3136, θ_{max} = 25.60°; reflections collected/unique: 37637/6668 [R(int) = 0.0403], R_1 ($I > 2\sigma(I)$) = 0.0399, wR_2 ($I > 2\sigma(I)$) = 0.0945. X-ray intensity data were measured at 123 K on a Bruker SMART APEX CCD-based diffractometer (Mo Kα radiation, λ = 0.71073 Å). The raw frame data were integrated into SHELX-format reflection files and corrected for Lorentz and polarization effects using SAINT.[9] Corrections for incident and diffracted beam absorption effects were applied using SADABS.[9] None of the crystals showed evidence of crystal decay during data collection. The structure was solved by a combination of direct methods and difference Fourier syntheses and refined against F^2 by the full-matrix least-squares technique. Crystallographic data (excluding structure factors) for the structure reported in this paper have been deposited with the Cambridge Crystallographic Data Center as supplementary publication no CCDC 857538. Copies of the data can be obtained free of charge on application to CCDC, 12 Union Road, Cambridge CB2 1EZ, U.K. (fax: (+44)1223-336-033; e-mail: deposit@ccdc.cam.ac.uk).

■ ASSOCIATED CONTENT

Ⓢ Supporting Information

Crystallographic data in CIF format. Further details are given in Figures S1−S21. This material is available free of charge via the Internet at http://pubs.acs.org.

■ AUTHOR INFORMATION

Corresponding Author

*E-mail: yubindong@sdnu.edu.cn

Notes

The authors declare no competing financial interest.

■ ACKNOWLEDGMENTS

This work was supported by NSFC (Nos. 91027003 and 21072118), 973 Program (No. 2012CB821705), "PCSIRT", Shangdong Natural Science Foundation (No. JQ200803), and Taishan scholars' construction project special fund.

■ REFERENCES

(1) (a) Li, M.; Selvin, P. *J. Am. Chem. Soc.* **1995**, *117*, 8132. (b) Tremblay, M. S.; Sames, D. *Chem. Commun.* **2006**, 4116. (c) Faulkner, S.; Pope, S. *J. Am. Chem. Soc.* **2003**, *125*, 10526. (d) Poole, R. A.; Kielar, F.; Richardson, S. L.; Stenson, P. A.; Parker, D. *Chem. Commun.* **2006**, 4084. (e) Costes, J.-P.; Dahan, F.; Dupuis, A.; Laurent, J.-P. *Chem.—Eur. J.* **1998**, *4*, 1616. (f) Petoud, S.; Cohen, S. M.; Bünzli, J.-C. G.; Raymond, K. N. *J. Am. Chem. Soc.* **2003**, *125*, 13324. (g) Gonçalves e Silva, F. R.; Malta, O. L.; Reinhard, C.; Güdel, H.-U.; Piguet, C.; Moser, J. E.; Bünzli, J.-C. G. *J. Phys. Chem. A* **2002**, *106*, 1670−1677. (h) Bünzli, J.-C. G. *Chem. Rev.* **2010**, *110*, 2729. (i) Shavaleev, N. M.; Scopelliti, R.; Gumy, F.; Bünzli, J.-C. G. *Inorg. Chem.* **2008**, *47*, 9055. (j) Shavaleev, N. M.; Gumy, F.; Scopelliti, R.; Bünzli, J.-C. G. *Inorg. Chem.* **2009**, *48*, 5611. (k) Elhabiri, M.; Scopelliti, R.; Bünzli, J.-C. G.; Piguet, C. *J. Am. Chem. Soc.* **1999**, *121*, 10747. (l) Bünzli, J.-C. G.; Piguet, C. *Chem. Rev.* **2002**, *102*, 1897.

(2) (a) Deng, H. X.; Doonan, C. J.; Furukawa, H.; Ferreira, R. B.; Towne, J.; Knobler, C. B.; Wang, B.; Yaghi, O. M. *Science* **2010**, *327*, 846. (b) Cui, Y.; Yue, Y.; Qian, G.; Chen, B. *Chem. Rev.* **2012**, *112*, 1126. (c) Cohen, S. M. *Chem. Rev.* **2012**, *112* (2), 970. (d) Li, J.-R.; Sculley, J.; Zhou, H.-C. *Chem. Rev.* **2012**, *112*, 970. (e) Zhang, J.-P.; Zhang, Y,-B.; Lin, J.-B.; Chen, X.-M. *Chem. Rev.* **2012**, *112*, 1001. (f) Wu, H.; Gong, Q.; Olson, D. H.; Li, J. *Chem. Rev.* **2012**, *112*, 836. (g) Wang, C.; Zhang, T.; Lin, W. *Chem. Rev.* **2012**, *112*, 1084. (h) Horcajada, P.; Gref, R.; Baati, T.; Allan, P. K.; Maurin, G.; Couvreur, P.; Férey, G.; Morris, R. E.; Serre, C. *Chem. Rev.* **2012**, *112*, 1232. (i) Yoon, M.; Srirambalaji, R.; Kim, K. *Chem. Rev.* **2012**, *112*, 1196. (j) Suh, M. P.; Park, H. J.; Park, H. J.; Prasad, T. K.; Lim, D.-W. *Chem. Rev.* **2012**, *112*, 782. (k) Kreno, L. E.; Leong, K.; Farha, O. K.; Allendorf, M.; Van Duyne, R. P.; Hupp, J. T. *Chem. Rev.* **2012**, *112*, 1105. (l) Sumida, K.; Rogow, D. L.; Mason, J. A.; McDonald, T. M.; Bloch, E. D.; Herm, Z. R.; Bae, T-H.; Long, J. R. *Chem. Rev.* **2012**, *112*, 724.

(3) (a) Dong, Y.-B.; Jiang, Y.-Y.; Li, J.; Ma, J.-P.; Liu, F.-L.; Tang, B.; Huang, R.-Q.; Batten, S. R. *J. Am. Chem. Soc.* **2007**, *129*, 4520. (b) Jiang, Y.-Y.; Ren, S.-K.; Ma, J.-P.; Liu, Q.-K.; Dong, Y.-B. *Chem.—Eur. J.* **2009**, *15*, 10742.

(4) Ludwig, R. *Angew. Chem., Int. Ed.* **2001**, *40*, 1808.

(5) Hendrik, J.; Vreman, R.; David, K. *Pediatr. Res.* **1998**, *44*, 804.

(6) (a) Wang, P.; Ma, J.-P.; Dong, Y.-B.; Huang, R.-Q. *J. Am. Chem. Soc.* **2007**, *129*, 10620. (b) Dong, Y.-B.; Wang, P.; Ma, J.-P.; Zhao, X.-X.; Tang, B.; Huang, R.-Q. *J. Am. Chem. Soc.* **2007**, *129*, 4872. (c) Wang, P.; Ma, J.-P.; Dong, Y.-B. *Chem.—Eur. J.* **2009**, *15*, 10432.

(7) (a) Parker, D.; Dickins, R. S.; Puschmann, H.; Crossland, C.; Howard, J. A. K. *Chem, Rev.* **2002**, *102*, 1977. (b) Wolbers, M. P. O.; Veggel, F. C. J. M.; Snellink-Ruël, B. H. M.; Hofstraat, J. W.; Geurts, F. A. J.; Reinhoudt, D. N. *J. Am. Chem. Soc.* **1997**, *119*, 138. (c) Chappell, L. L.; Voss, D. A.; Horrocks, W. D.; Morrow, J. R. *Inorg. Chem.* **1998**, *37*, 3989. (d) Wong, K.-L.; Law, G.-L.; Yang, Y.-Y.; Wong, W.-T. *Adv. Mater.* **2006**, *18*, 1051.

(8) (a) An, J.; Shade, C. M.; Chengelis-Czegan, D. A.; Petoud, S.; Rosi, N. L. *J. Am. Chem. Soc.* **2011**, *133*, 1220. (b) Lan, Y.-Q.; Jiang, H.-L.; Li, S.-L.; Xu, Q. *Adv. Mater.* **2011**, *23*, 5015.

(9) Sheldrick, G. M. *SHELXTL*, Version 5.12; Bruker Analytical X-ray Systems, Inc.: Madison, WI, 1997.